Eccentricity Optimisation of Annular Multi-Tube Storage Unit with Phase Change Material

Yasser Harmen, Younes Chhiti, Maryam El Fiti, Mustapha Salihi, Charafeddine Jama

▶ **To cite this version:**

Yasser Harmen, Younes Chhiti, Maryam El Fiti, Mustapha Salihi, Charafeddine Jama. Eccentricity Optimisation of Annular Multi-Tube Storage Unit with Phase Change Material. SSRN : Social Science Research Network, 2022, SSRN Electronic Journal, 10.2139/ssrn.4220792 . hal-03784437

HAL Id: hal-03784437
https://hal.univ-lille.fr/hal-03784437v1

Submitted on 23 Sep 2022

HAL is a multi-disciplinary open access archive for the deposit and dissemination of scientific research documents, whether they are published or not. The documents may come from teaching and research institutions in France or abroad, or from public or private research centers.

L'archive ouverte pluridisciplinaire **HAL**, est destinée au dépôt et à la diffusion de documents scientifiques de niveau recherche, publiés ou non, émanant des établissements d'enseignement et de recherche français ou étrangers, des laboratoires publics ou privés.

Eccentricity optimisation of annular multi-tube storage unit with phase change material

Yasser Harmen[1,2*], Younes Chhiti[1,2], Maryam El Fiti[1,2], Mustapha Salihi[1,2], Charafeddine Jama[3]

[1] *Mohammed VI Polytechnic University, Ben Guerir, Morocco*
[2] *Laboratoire des Matériaux avancés et de Génie des Procédés, École nationale supérieure de chimie, Ibn Tofail University, Kenitra, Morocco*
[3] *University of Lille, CNRS, INRAE, Centrale Lille, UMR 8207, UMET-Unité Matériaux et Transformations, F-59000 Lille, France*

* Corresponding author: Yasser.harmen@um6p.ma

ABSTRACT

Thermal energy storage (TES) with phase change materials (PCM) can improve energy efficiency by reducing energy availability and demand mismatch. However, despite the potential of this technology, the low thermal conductivity of PCM slows down the storage cycle and limits its commercialisation. The literature has proposed many solutions to improve heat transfer, such as fins, encapsulation, or metal foam inserts, which are too expensive and complicated. This study focuses on an inexpensive and practical solution, eccentricity of shell and tube heat exchanger (STHE). The eccentricity of four horizontal STHE with 1, 2, 3, and 4 tubes is studied. The PCM melting and solidifying characteristics with varied eccentricities are accurately predicted by the enthalpy double porosities model. Results reveal that the eccentric charge performance is better than the concentric arrangement of the tube. An optimal eccentricity of the charge cycle exists that depends on the tube. The optimal eccentricities of the single and multi-tube systems are 6 and 10. The total melting time of optimal eccentricity for the four-tube, three-tube, two-tube, and single-tube is optimised by 63%,63%, 60% and 54% compared to the concentric cases, respectively. The optimal eccentricity of the single-tube case has the shortest melting time, which increases linearly with the Rayleigh number. The concentric cases consistently exhibit the best performance and shortest solidification time as the Rayleigh number increases. The total solidification time of the single-tube case is reduced by 56%, 52% and 49% compared to the four-tube, three-tube and two-tube, respectively. The multiphysical mechanisms of the charge and discharge cycles are discussed. Special attention is paid to understanding the melting and solidification behaviour.

Keywords: Thermal energy storage; Phase change material; Computational fluid dynamics; Heat transfer enhancement; Eccentricity

Electronic copy available at: https://ssrn.com/abstract=4220792

Nomenclature

C_p: Specific heat ($J.kg^{-1}.K^{-1}$)

A(f): Porosity function

C_{mush}: Mushy zone constant ($kg.m^{-3}.s^{-1}$)

τ : Fourier number

g: Acceleration of gravity ($m.s^{-2}$)

L: Latent heat of fusion ($J.g^{-1}$)

Ra: Rayleigh number

ref: Reference

T: Temperature (K)

t: Time (s)

u, v: x and r velocity components ($m.s^{-1}$)

x, y: Cartesian coordinates (m)

Greek

λ: Thermal conductivity ($W.m^{-1}.K^{-1}$)

μ: Kinetic viscosity ($kg.m^{-1}.s^{-1}$)

ρ: Density ($kg.m^{-3}$)

β: Thermal expansion coefficient (K^{-1})

φ: Eccentricity

Subscripts

f: Melting fraction

i: Initial

in: Inner tube

m: Melting

opt: Optimal

out: Outer tube

s: Solidification

δ: small constant number

List of abbreviations

CFD: Computational fluid dynamics

HTF: Heat transfer fluid

LTES: Latent thermal energy storage

PCM: Phase change materials

PCT: Phase change temperature

STHE: Shell and tube heat exchanger

Electronic copy available at: https://ssrn.com/abstract=4220792

1. Introduction

Thermal energy storage (TES) is a promising technology that can help develop future efficient and environmentally friendly energy systems to achieve a more regular, effective, stable and 24-hour energy supply from renewables. TES can be classified according to three physical phenomena: sensible enthalpy variation, phase change enthalpy and reversible reaction. The latent TES (LTES) system with phase change materials (PCM) stores and releases a high amount of energy during the charge and discharge cycles (Harmen et al., 2020). Therefore, LTES garnered interest in various sectors, especially for heating, electricity, and higher applications.

The shell and tube heat exchanger (STHE) is the preferred technology for LTES. This is due to its good compromise between thermal performance, compactness, implementation complexity, cost and industrial maturity (Wazeer et al., 2022)(Trp et al., 2006). Furthermore, it is a flexible and adaptable technology that achieves high-capacity factors and interesting power densities (Medrano et al., 2009). A prerequisite for developing and applying these systems is improving heat transfer in PCM-based systems. Along with these, energy scientists and technologists are working to improve the LTES systems' performance. The performance enhancement methods can be classified into four categories : (1) enhancing PCM thermal conductivity, such as through filled PCM into porous media (Zhang et al., 2021) and adding nanomaterials (Sun et al., 2020), (2) extending heat transfer surface with finned tubes (El Fiti et al., 2022) and encapsulated PCM (Hu et al., 2022) and (3) improving uniformity of heat transfer process by exploring efficient storage unit orientations (Harmen et al., 2021), eccentricity optimisation (Yao and Chen, 1980) and optimise the operating parameters (Mekrisuh et al., 2020). The third method is a simpler, most economical and practical approach to enhancing LTES systems' performance. These simple solutions are reviewed and discussed in the following.

Recent studies have shown that the storage unit orientation considerably impacts the melting and solidification performance. Mehta et al. (Mehta et al., 2019a) show that the horizontal orientation offers a faster storage time. In contrast, Kalapala et al. (Kalapala and Devanuri, 2020) reveal that the storage cycle is faster for the vertical configuration. In addition, previous surveys have found that the inclined setting is better than the vertical and horizontal cases (Mehta et al., 2019b). In our previous study, the optimal configuration depends on the heat transfer fluid (HTF) flow rate and the tube/shell diameter ratio (Harmen et al., 2021). Assuming

Electronic copy available at: https://ssrn.com/abstract=4220792

the horizontal orientation is the best performing, it can be further improved by adjusting the relative positions of the tubes and shell, i.e., the eccentricity parameter.

Pahamli et al. (Pahamli et al., 2016) numerically examined the influence of eccentricity on the melting of paraffin-filled single-tube LTES unit. Shell and tube diameters were taken as 60 mm and 10 mm, and the tube is offset downwards out of the centre on three levels e = 7.5, 15 and 22.5 mm. The results reveal that increasing eccentricity reduces melting time by 33, 57 and 64% as the eccentricity increases from 7.5 mm to 22.5 mm. Yazici et al. (Yazici et al., 2014) carried out an experimental analysis on the solidification of paraffin placed in the eccentric annulus. The tube was moved eccentrically upward and downward; five different eccentricity values are considered: e = -10, -20, -30, 10, 20 and 30 mm. They reported that upward or downward eccentricity increased the total discharge time. Zheng et al. (Zheng et al., 2018) revealed the existence of an optimal eccentricity for the shortest charge time, i.e., increasing the eccentricity does not systematically ensure a higher charging performance. Unlike melting, the solidification time increases as eccentricity increases. However, these conclusions are relative due to the approach adopted in this work, which does not involve formal optimisation methods to predict optimal geometry. More recently, Kadivar et al. (Kadivar et al., 2019) carried out a numerical analysis to investigate the effect of the radial and tangential eccentricities on the melting and solidifying of N-eicosane. This study extends the research of Zheng et al. (Zheng et al., 2018) by using a surface-based formal optimisation approach to optimise the storage time. The quickest configuration, 7.1 times faster than the concentric one, is obtained with radial and tangential eccentricities of 0.841 and 0.029π. The slowest configuration, 3.6 times slower than the concentric case, is obtained with radial and tangential eccentricities of 0.999 and π. Although the solidification process is faster in the concentric case. Also, they proved that the shell-to-tube diameter ratios has no noticeable effect on the optimisation outcomes.

According to the above discussion, it is found that the eccentricity of the horizontal shell and tube is an inexpensive and practical solution to reduce the charge time and augment the discharge time. Nevertheless, it remains unknown whether an optimal eccentricity value exists to obtain the highest charging or charging-discharging results for multiple tubes. Indeed, this is the first research conducted on the eccentricity of a shell and tubes LTES with 1, 2, 3 and 4 tubes. Thus, this study focuses on the optimal eccentricity of the four units, to not enough

Electronic copy available at: https://ssrn.com/abstract=4220792

attention has been paid so far. The following sections present and discuss the model, methods and details of the results.

2. Problem statement

2.1. Physical model

The LTES system involves the melting and solidification process in a horizontal STHE. The HTF flows into the tube and PCM in the annular space. A simplified two-dimensional model is adopted because the length/shell diameter ratio is usually significant (see **Figure 1**). The tube and the shell thickness are 1 mm and 2 mm. The outer shell is thermally insulated. The base case includes one tube and shell with an inner diameter of 20 and 40 mm.

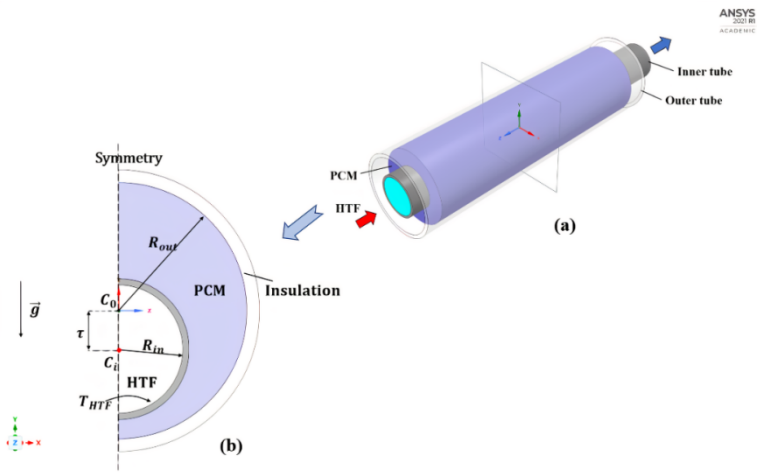

Figure 1: Three-dimensional schematic of the physical model: horizontal single-tube LTES unit (a) and two-dimensional diagram of the computational model (b).

The variable φ refers to the axial distance between the tube centre and the shell centre (radial eccentricity). The tube is positioned vertically up or down from the shell centre. The tangential eccentricity of the tube is neglected. The four configurations studied in this section are shown in **Figure 2**.

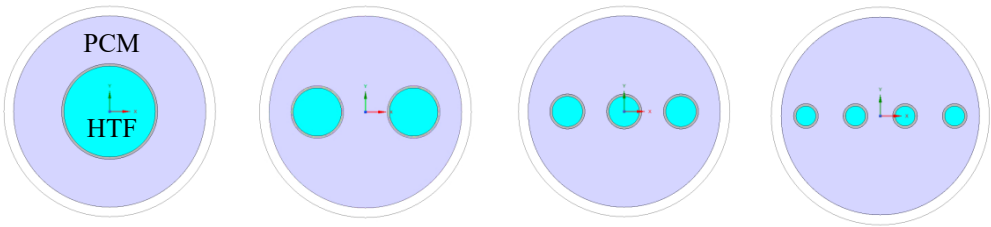

Figure 2: Physical models: configuration a: single-tube, configuration b: two-tube, configuration c: three-tube and configuration d: four-tube.

Electronic copy available at: https://ssrn.com/abstract=4220792

The PCM amount is fixed for all the studied cases; tube diameters are set according to the number of tubes. The aim is to provide optimal combinations of eccentricity and tube number to improve storage performance.

2.2. Mathematical formulation

The LTES model was developed based on energy and Navier-Stokes equations, including conduction heat transfer and natural convection. The phase change is modelled using the enthalpy-porosity method (Voller and Prakash, 1987). The porosity factor represents the volume percentage of the liquid PCM allocated to each computing domain cell. The following assumptions are made: (1) the liquid PCM is an incompressible laminar Newtonian fluid, and viscous dissipation is neglected, (2) The buoyancy force is calculated using the Boussinesq approximation (**Equation 5**), (3) heat loss to the environment is ignored. The governing equations for transient laminar flow involving Boussinesq approximation are given as:

- **Mass conservation equation:**

$$\frac{\partial u}{\partial x}+\frac{\partial v}{\partial y}=0 \qquad \textit{Eq. 1}$$

- **Momentum conservation equations:**

$$\rho\left(\frac{\partial u}{\partial t}+u\frac{\partial u}{\partial x}+v\frac{\partial u}{\partial y}\right)=\mu\left(\frac{\partial^2 u}{\partial x}+\frac{\partial^2 u}{\partial y}\right)-C_{mush}\frac{(1-f)^2}{f^2+\delta}u \qquad \textit{Eq. 2}$$

$$\rho\left(\frac{\partial v}{\partial t}+u\frac{\partial v}{\partial x}+v\frac{\partial v}{\partial y}\right)=\mu\left(\frac{\partial^2 v}{\partial x}+\frac{\partial^2 v}{\partial y}\right)+C_{mush}\frac{(1-f)^2}{f^2+\delta}v+\rho_{ref}g\beta(T-T_{ref}) \qquad \textit{Eq. 3}$$

$$\begin{cases} f=1\ T<T_m\ \text{solid} \\ 0<f<0\ \text{mushy} \\ f=1\ T>T_m\ \text{liquid} \end{cases} \qquad \textit{Eq. 4}$$

$$(\rho-\rho_{ref})=-\rho_{ref}g\beta(T-T_{ref}) \qquad \textit{Eq. 5}$$

The third term on the right of **Equation 2** and **Equation 3** is the porosity function (A(f)) defined by Brent et al. (Brent et al., 1988). A(f) describes the front between the solid and liquid PCM. The local melting fraction, f, is computed using **Equation 4**. C_{mush} is the mushy zone factor, reflecting the morphology of the phase change front, and it equals 10^5 $kg.m^{-3}.s^{-1}$. δ is a small value (0.01) to prevent the division by zero when the PCM is solid.

- **Energy equation:**

Electronic copy available at: https://ssrn.com/abstract=4220792

$$\frac{\partial}{\partial t}\left((\rho c_p)_{PCM}\right) + \rho_{PCM} L \frac{\partial f}{\partial t} + (\rho c_p)_{PCM}\left(u\frac{\partial T}{\partial x} + v\frac{\partial T}{\partial y}\right) = \lambda_{PCM}\left(\frac{\partial^2 T}{\partial x^2} + \frac{\partial^2 T}{\partial y^2}\right) \quad (6)$$

2.3. Numerical model settings

The above partial differential governing equations were solved numerically using the control volume approach provided by the commercial CFD software ANSYS-Fluent 19. The SIMPLE algorithm is used for treating the pressure-velocity coupling. The PRESTO (PREssure STaggering Option) scheme was adopted for the pressure correction equation. The QUICK differencing scheme performs the discretisation of the momentum and energy equations. The second upwind technique is used to discretize the convective components. The under-relaxation factors for density, pressure, velocity and liquid fraction were 0.7, 0.2, 0.4 and 0.9. During the iterative process, the residual tolerances for the conservation of mass, momentum, and energy equations were checked every time step and were assumed to be 10^{-7}, 10^{-7} and 10^{-10}, respectively. Simulations were conducted on Dell Precision 3630 Tower computer, consisting of seven compute nodes, each with two six-core Intel Westmere Xeon X5650CPUs and 32 GB of memory. The complete melt or solidification requires between 30 and 50 hours of computation.

2.4. PCM thermal and physical properties and boundary conditions

Paraffin with a phase change temperature (PCT) point of 328 K is used as PCM. The temperature dependence of the thermal and physical properties besides density has been ignored. The thermal and physical properties of paraffin are derived from our previous work (Harmen et al., 2021). The initial boundary conditions are modelled using:

- The tube wall boundary: constant temperature condition and no-slip velocity. $u = v = 0$, $T = T_i$.
- The outer shell wall boundary: no-slip velocity and adiabatic condition. $u = v = 0$, $\frac{\partial T}{\partial x} = \frac{\partial T}{\partial y} = 0$.

The paraffin is initially subcooled or superheated by 2 K for the melting or solidification. The tube temperature is 16 K above the initial charge temperature and 16 K under the initial discharge temperature.

Electronic copy available at: https://ssrn.com/abstract=4220792

2.5. Independency study and model validation

The numerical model is validated with experimental data and numerical results. Indeed, it is subject to rigorous independent testing to ensure satisfactory accuracy and relatively low run time. Initially, a mesh and time step convergence study is performed to validate the spatial and temporal convergence. The physical model is discretised over three selected mesh sizes (0.1 mm, 0.2 mm and 0.4 mm) and three steps (0.05 s, 0.1 s and 0.2 s) to find the most suitable element size-time step combination. At t = 1000 s (with a time step of 0.1 s), the liquid fraction predicted by the three mesh systems is presented in **Figure 3(a)**. It can be verified that a sufficiently smooth melting front is obtained with small grid sizes. **Figure 3(b)** gives the evolution of the melting fraction with time for the three-time steps when the grid size is 0.1 mm.

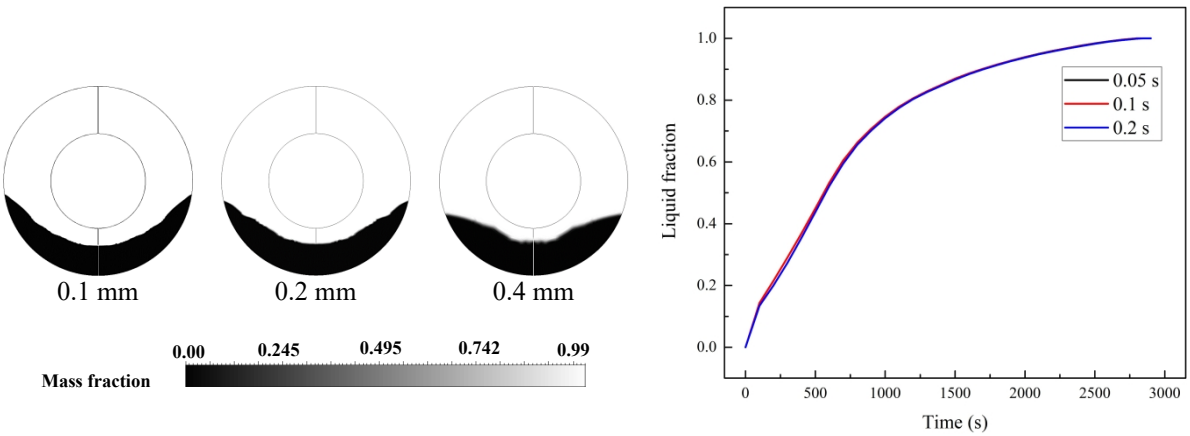

Figure 3: Liquid fraction for three grid systems at 1000 s (a) and evolution of the liquid fraction versus time for different time steps (b).

The model's ability to predict the charge cycle is experimentally validated. The case simulated is similar to that reported by Dhaidan et al. (Dhaidan et al., 2013). The system consists of a 16.1 mm diameter aluminium tube inside a 44.5 mm Plexiglas shell. The storage unit is mounted horizontally with the paraffin as PCM contained in the annular space. The system was initially sub-cooled by 5.3 K, and a heat flow of 1821.3 W.m^2 was applied to the tube surface. The thermal and physical properties of PCM, HTF, aluminium and Plexiglas can be found in (Dhaidan et al., 2013)(Kousha et al., 2017). **Figure 4** compares the numerical predictions of this study and the experimental and numerical results of Dhaidan et al. (Dhaidan et al., 2013). This figure compares the temporal evolution of the melting front. The experimental melting of the PCM was monitored by tracking the temporal progression of the melting front shape

Electronic copy available at: https://ssrn.com/abstract=4220792

visually. The approach used in this work accurately predicts the buoyancy-driven flow of the liquid PCM in an annular LTES.

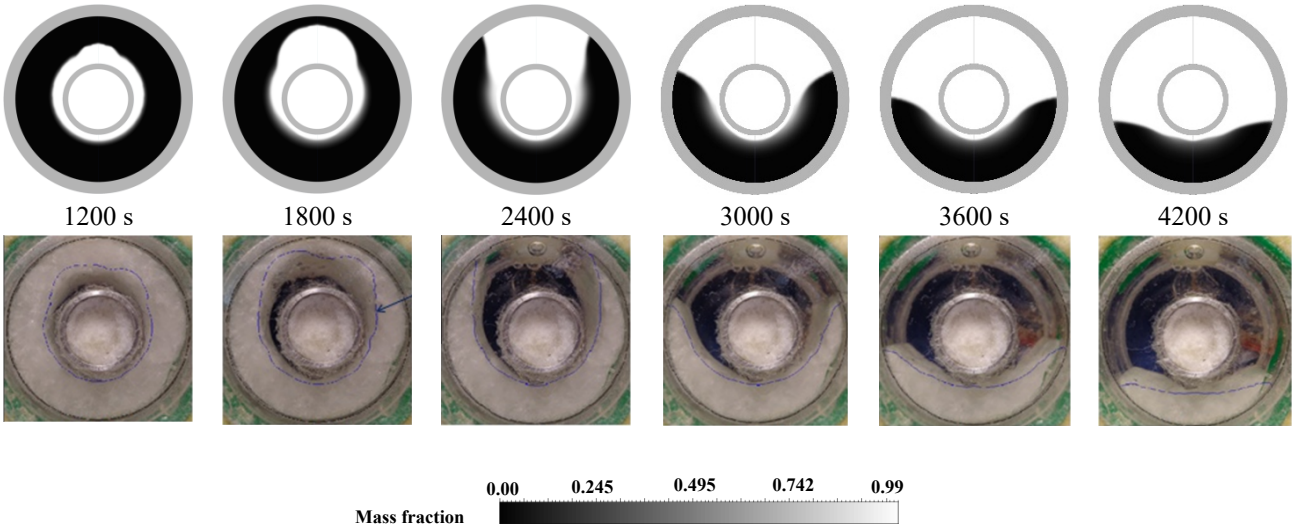

Figure 4: Validation of the numerical model for the melting process in a horizontal single-pass STHE unit. The numerical results of this study appear at the top, while the experimentally visualized and numerically predicted (blue line) melting fronts from Ref. (Dhaidan et al., 2013) *are on the bottom.*

The proposed model accuracy is verified for the discharge cycle. The temporal evolution of the numerical solidification front is compared with experiments of Assis et al. (Assis et al., 2008) (**Figure 5**).

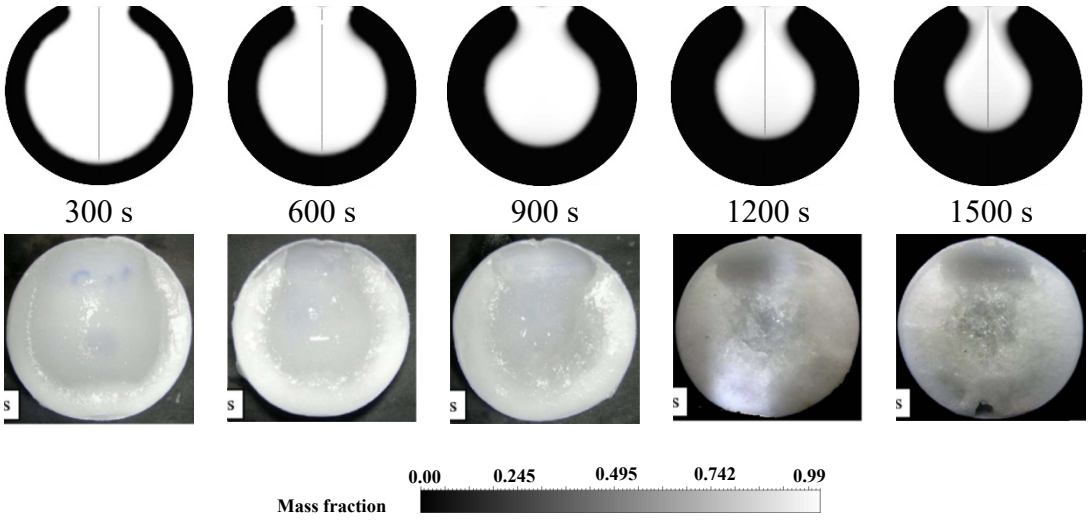

Figure 5: Validation of the numerical model for the solidification process in a spherical shell. The numerical results of this study appear at the top, and the experimental fronts in Ref. (Assis et al., 2008) *are at the bottom.*

Paraffin wax with a melting temperature of 28 °C is contained in a plastic spherical shell of 40 cm. Solidification is carried out by emerging the PCM into a circulating thermostatic bath

Electronic copy available at: https://ssrn.com/abstract=4220792

maintained at 20 °C below the PCT. A noticeable difference between the two results is observed at the upper layer due to the PCM-air interaction. Our model does not consider this effect because of its huge computational cost. Overall, the enthalpy-porosity method predicts the shape and temporal evolution of the melting and solidification fronts. Hence, it can be confidently used for the optimisation study presented in the following sections.

3. Results and discussion

3.1. Charging process

Figure 6 gives the total melting time versus tube eccentricity. The total charge time is defined by the non-dimensional Fourier number (τ) (Bergman Lavine, Adrienne S., Incropera, Frank P., DeWitt, David P., 2017). The possible positive and negative eccentricities are investigated by moving the tube in 2 mm increments. Negative values correspond to the upper position of the tube, while the positive values correspond to the bottom location.

The eccentricity parameter significantly influences the total melting time, and an optimal value exists. Indeed, negative values decrease the storage performance; charge time increases as eccentricity decreases. Interestingly, positive eccentricity improves the charge performance by reducing the total melting time. The melting time of the single-tube system is much lower than that of the multi-tube systems for respective eccentricity values. The optimal eccentricity of the multi-tube system is 10 instead of 6 for the single-tube. The total melting time of optimal eccentricity for the four-tube, three-tube, two-tube and single-tube are 1750 s, 1700 s, 1600 s and 1300 s. Hence, 63%, 63%, 60% and 54% of the charge time is optimised compared to the concentric case of the four configurations, respectively.

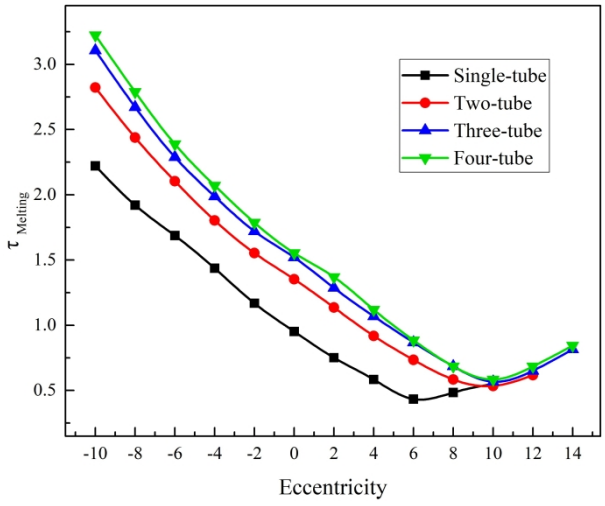

Figure 6: Effect of eccentricity on total melting time for single and multi-tube systems.

Electronic copy available at: https://ssrn.com/abstract=4220792

The fields of liquid fraction, temperature, and velocity are presented to explain the existence of an optimal eccentricity (**Figure 7**). Seven cases are presented: reference case of the single-tube (concentric case without natural convection), baseline case of the single-tube (concentric case with natural convection), $\varphi = 6$ case of the single-tube (quickest melting rate), $\varphi = -10$ case of the single-tube (slowest melting rate) and $\varphi = 10$ case of multi-tube (quickest melting rate of multi-tube systems). For the reference case, the PCM melts symmetrically to the tube. The total melting time of the baseline case is 4% higher than the reference case. Thus, natural convection improves the performance of the charge cycle and affects the behaviour of the melting front.

Regarding the baseline case, the PCM melting process is divided into four successive phases: conduction dominant, convection dominant, conduction+convection dominant and conduction dominant. The first phase is the shortest (100 s) and leads to melting a thin layer (15% of the PCM) around the tube by heat conduction, as in the reference case. Next, the melting of the upper part is accelerated by the dominance of natural convection. The buoyancy-driven flow circulates the liquid PCM from the lower to the upper layers. Two convection cells are observed: a main axial cell that ensures the upper axial melting and a radial cell that ensures the tangential melting. These prevent stratification of the temperature distribution; thereby, the temperature of the molten PCM is uniform. Hence, the melting front advances obliquely. This phase is shown between $\tau = 0.0668$ and $\tau = 0.2672$, and 50% of the PCM is melted (**Figure 7**). The convection+conduction phase is characterised by the onset of thermal stratification and the decrease of the melting rate by weak convective effects. This phase starts at $\tau = 0.3340$, the magnitude of buoyancy-driven decreases and three temperature levels are observed (orange, yellow and green). The last phase is marked by conduction; the charging rate is significantly reduced ($\tau = 0.4008$). This phase starts with 20% solid PCM. However, it takes 58% of the total melting time. The four phases are confirmed by our previous experimental and numerical results (Harmen et al., 2021)(El Fiti et al., 2022), where four phases are identified: slow charge, very fast charge, fast charge and very slow charge.

The four phases are still observed in all other cases of multi-tube systems but with different kinetics. Based on the above analysis, shifting the tube downwards reduces the charge time. In contrast, moving the tube to the upper part increases the total melting time; more than 70% of the PCM is melted in phase 4. For positive eccentricity cases, the PCM amount below the tube is reduced; hence, phases 3 and 4 are almost eliminated. Indeed, PCM is melted mainly by thermal convection. Nevertheless, a higher eccentricity often does not lead to a greater melting

Electronic copy available at: https://ssrn.com/abstract=4220792

rate. The optimal value is a synergy of the four phases to ensure a fast melting of the upper and lower parts. In the φ = 6 case, small equal solid fractions remain on both sides and melt simultaneously. However, in φ = 8 and φ = 4 cases, the upper and lower part of the PCM limit the total melting, respectively.

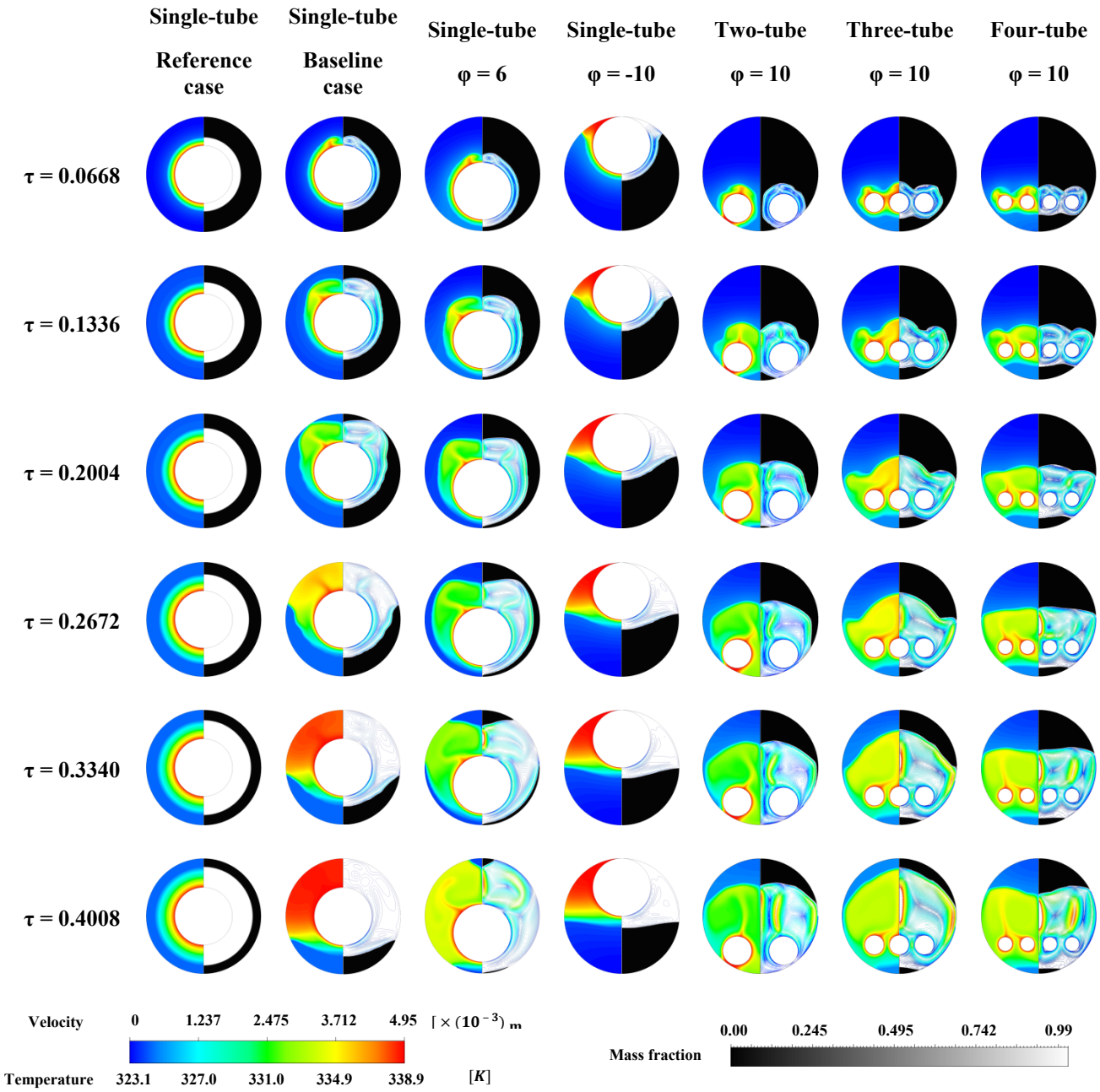

Figure 7: Melting fraction, temperature, and velocity filed of the reference case of the single-tube (concentric case without natural convection), baseline case of the single-tube (concentric case with natural convection), φ = 6 case of the single-tube (quickest melting rate), φ = -10 case of the single-tube (slowest melting rate) and φ = 10 cases of multi-tube (quickest melting rate).

Electronic copy available at: https://ssrn.com/abstract=4220792

As discussed above, the melting process is highly sensitive to the ratio of natural convection to thermal conduction. This ratio can be described by the non-dimensional Rayleigh number, equal to 1.25×10^6 in all studied cases. Indeed, a higher Rayleigh number will increase the optimal eccentricity and vice versa. **Figure 8** shows the optimal eccentricity of the single-tube configuration for three different Rayleigh numbers. As illustrated, the optimal eccentricity increases linearly with the Rayleigh number by decreasing the melting time. This relationship can be expressed as: $\tau_{\mathrm{opt}} = 5.6 + 3.2 \times 10^{-7} * \mathrm{Ra}$.

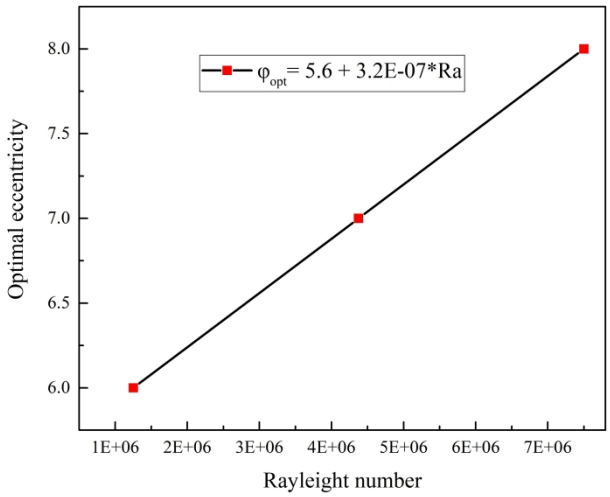

Figure 8: Rayleigh number effect on the optimal eccentricity of the single-tube configuration.

3.2. Discharging process and charge-discharge cycle

Figure 9 illustrates the total non-dimensional solidification time as a function of tube eccentricity. Unlike the charge cycle, eccentricity increases the discharge time. The concentric case is advantageous in the solidification process. The total solidification time of optimal eccentricity for the four-tube, three-tube, two-tube, and the single-tube is 11150 s, 10400 s, 9600 s and 4900 s. The negative eccentricity is of particular interest compared to the positive one. This effect suggests that the discharge and charge mechanisms are different.

Electronic copy available at: https://ssrn.com/abstract=4220792

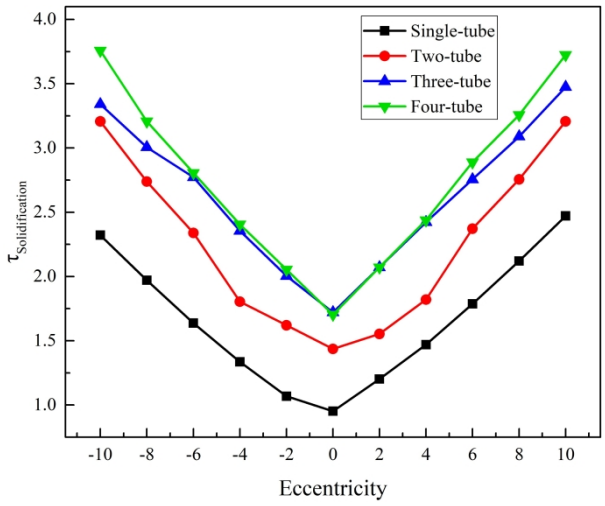

Figure 9: Effect of eccentricity on total solidification time for single and multi-tube systems.

The solidification fraction, temperature field and velocity vectors for the reference, base, φ = 6 and φ = -10 cases are shown in **Figure 10**. Seven cases are presented: reference case of the single-tube, baseline case of the single-tube (quickest solidification rate), φ = 6 case of the single-tube (quickest melting rate), φ = -10 case of the single-tube (slowest melting rate) and φ = 0 cases of multi-tube (quickest solidification rate).

The discharge behaviour of the reference case is similar to the charge cycle. The solidification front advances uniformly towards the shell. The solidification cycle is divided into three stages in the baseline case: conduction dominant, conduction+convection dominant, and conduction dominant. Phase 1 is faster than the second and third phases, where a thin layer of solid PCM appears. Next, the solidification is mainly governed by conduction and weak convection throughout the liquid PCM (τ = 0.0668). This leads to a hot liquid PCM at the upper part and a cold liquid PCM at the lower part. Hence, the lower part has a higher solid fraction than the upper part. The natural convection disappears once liquid PCM reaches the PCT (τ = 0.2004). Phase 3 limits the total discharge as weak conduction dominates. The upper part solidifies last due to the buoyancy-driven recirculation observed in phase 2 (τ = 0.8350). This is because the natural convection cells accelerate the solidification of the lower part. Hence, the eccentricity of the upper side allows quick solidification compared to the corresponding lower cases. The three stages are still observed in all other cases of multi-tube systems but with different kinetics.

Electronic copy available at: https://ssrn.com/abstract=4220792

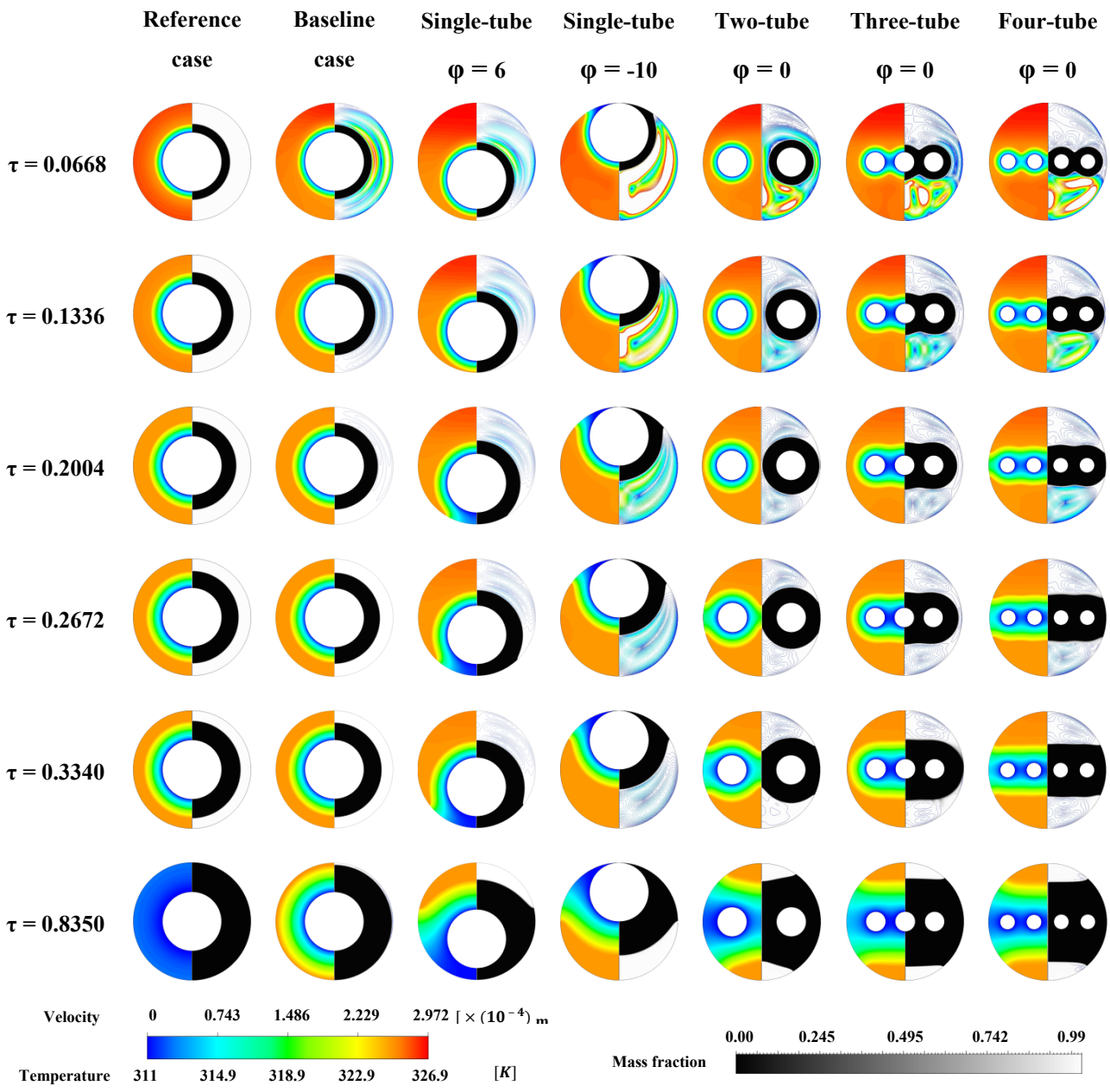

Figure 10: Solidification fraction, temperature, and velocity field of a single-tube of the reference case of the single-tube, baseline case of the single-tube (quickest solidification rate), φ = 6 case of the single-tube (quickest melting rate), φ = -10 case of the single-tube (slowest melting rate) and φ = 0 cases of multi-tube (quickest solidification rate).

Figure 11 shows the combined charge and discharge cycle of the baseline case of the single-tube (quickest solidification rate), φ = 6 case of the single-tube (quickest melting rate) and φ = -10 case of the single-tube (slowest melting rate). The storage cycle of case φ = 6 is limited by the solidification time, which is higher than the melting time by 80%. The slowest melting rate

Electronic copy available at: https://ssrn.com/abstract=4220792

(φ = -10) has the slowest storage cycle, with a total Fourier number of 4.6. In contrast to the charge, increasing the Rayleigh number does not affect the optimal eccentricity.

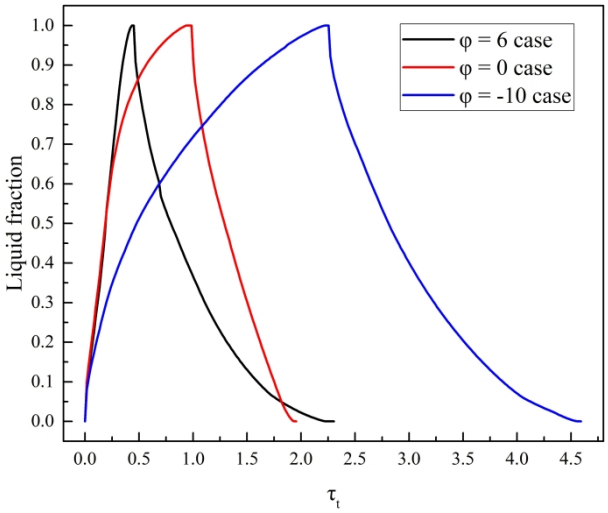

Figure 11: Melting and solidifying process of φ = 0 case (baseline case), φ = 6 case (quickest melting rate) and φ = -10 case (slowest melting rate).

The baseline case consistently exhibits the best performance and shortest solidification time as the Rayleigh number increases. Indeed, the eccentric configuration is suitable for applications with fast melting and slow solidification times, such as for building.

Conclusions

In this work, a numerical study was conducted to examine the effect of eccentricity on improving the melting-solidification performance. The storage unit is a horizontal shell and tubes PCM storage unit. The paraffin is used as PCM with a PCT of 325 K. The numerical analysis is performed using a porous fixed-grid model to provide an accurate prediction of the storage performance. The simulations are conducted on a two-dimensional physical model using the enthalpy-porosity method. The numerical model has been validated experimentally. The results show that eccentricity has a significant effect on storage performances. Positive values improve the charge performance by reducing the total melting time. The charge time of optimal eccentricities is optimised by 63%, 63%, 60%, and 54% compared to the concentric case of four-tube, three-tube, two-tube, and single-tube. The optimal melting time of the single-tube case is reduced by 26%, 24%, and 19% compared to the four-tube, three-tube, and two-tube. Also, the optimal eccentricity of the single-tube case increases as the Rayleigh number increases, given by $5.6 + 3.2 \times 10^{-7} * \mathrm{Ra}$. The PCM melting process is divided into four successive phases: conduction dominant, convection dominant, conduction+convection dominant and conduction dominant. In contrast, the concentric case has the shortest

Electronic copy available at: https://ssrn.com/abstract=4220792

solidification time of all cases. The total solidification time of the single-tube case is reduced by 56%, 52% and 49% compared to the four-tube, three-tube and two-tube, respectively. The solidification cycle is divided into three stages: conduction dominant, conduction and convection dominant, and conduction dominant. As well, increasing the Rayleigh number does not affect the optimal eccentricity. The concentric case presents the fast charge-discharge cycles. In future investigations, further study must be carried out to optimise the total charge-discharge cycle by combining several methods, i. e., fins and eccentricity.

References

Assis, E., Ziskind, G., Letan, R., 2008. Numerical and Experimental Study of Solidification in a Spherical Shell. J. Heat Transfer 131. https://doi.org/10.1115/1.2993543

Bergman Lavine, Adrienne S., Incropera, Frank P., DeWitt, David P., T.L., 2017. Fundamentals of Heat and Mass Transfer.

Brent, A.D., Voller, V.R., Reid, K.J., 1988. Enthalpy-porosity technique for modeling convection-diffusion phase change: Application to the melting of a pure metal. Numer. Heat Transf. https://doi.org/10.1080/10407788808913615

Dhaidan, N.S., Khodadadi, J.M., Al-Hattab, T.A., Al-Mashat, S.M., 2013. Experimental and numerical investigation of melting of NePCM inside an annular container under a constant heat flux including the effect of eccentricity. Int. J. Heat Mass Transf. https://doi.org/10.1016/j.ijheatmasstransfer.2013.08.002

El Fiti, M., Salihi, M., Harmen, Y., Chhiti, Y., Chebak, A., M'Hamdi Alaoui, F.E., Achak, M., Bentiss, F., Jama, C., 2022. Energetic performance optimization of a coaxial phase change material (PCM) regenerator. J. Energy Storage 50, 104571. https://doi.org/https://doi.org/10.1016/j.est.2022.104571

Harmen, Y., Chhiti, Y., Alaoui, F.E.M., Bentiss, F., Elkhouakhi, M., Deshayes, L., Jama, C., Duquesne, S., Bensitel, M., 2020. Storage efficiency of paraffin-LDPE-MWCNT phase change material for industrial building applications, in: 2020 5th International Conference on Renewable Energies for Developing Countries (REDEC). pp. 1–6.

Harmen, Y., Chhiti, Y., M'Hamdi Alaoui, F.E., Bentiss, F., El Khouakhi, M., Jama, C., Duquesne, S., Bensitel, M., Deshayes, L., 2021. Thermal and energetic behaviour of solid-solid-liquid phase change materials storage unit: Experimental and numerical comparative study of the top, bottom and horizontal configurations. J. Energy Storage

Electronic copy available at: https://ssrn.com/abstract=4220792

33, 102025. https://doi.org/https://doi.org/10.1016/j.est.2020.102025

Hu, M.-H., Xu, T., Chiu, J.N.W., 2022. Experimental analysis of submerged coil and encapsulated slab latent heat storage. Appl. Therm. Eng. 209, 118259. https://doi.org/https://doi.org/10.1016/j.applthermaleng.2022.118259

Kadivar, M.R., Moghimi, M.A., Sapin, P., Markides, C.N., 2019. Annulus eccentricity optimisation of a phase-change material (PCM) horizontal double-pipe thermal energy store. J. Energy Storage. https://doi.org/10.1016/j.est.2019.101030

Kalapala, L., Devanuri, J.K., 2020. Energy and exergy analyses of latent heat storage unit positioned at different orientations – An experimental study. Energy. https://doi.org/10.1016/j.energy.2020.116924

Kousha, N., Hosseini, M.J., Aligoodarz, M.R., Pakrouh, R., Bahrampoury, R., 2017. Effect of inclination angle on the performance of a shell and tube heat storage unit – An experimental study. Appl. Therm. Eng. https://doi.org/10.1016/j.applthermaleng.2016.10.203

Medrano, M., Yilmaz, M.O., Nogués, M., Martorell, I., Roca, J., Cabeza, L.F., 2009. Experimental evaluation of commercial heat exchangers for use as PCM thermal storage systems. Appl. Energy. https://doi.org/10.1016/j.apenergy.2009.01.014

Mehta, D.S., Solanki, K., Rathod, M.K., Banerjee, J., 2019a. Thermal performance of shell and tube latent heat storage unit: Comparative assessment of horizontal and vertical orientation. J. Energy Storage. https://doi.org/10.1016/j.est.2019.03.007

Mehta, D.S., Solanki, K., Rathod, M.K., Banerjee, J., 2019b. Influence of orientation on thermal performance of shell and tube latent heat storage unit. Appl. Therm. Eng. https://doi.org/10.1016/j.applthermaleng.2019.113719

Mekrisuh, K. u., Singh, D., Udayraj, 2020. Performance analysis of a vertically oriented concentric-tube PCM based thermal energy storage system: Parametric study and correlation development. Renew. Energy. https://doi.org/10.1016/j.renene.2019.10.074

Pahamli, Y., Hosseini, M.J., Ranjbar, A.A., Bahrampoury, R., 2016. Analysis of the effect of eccentricity and operational parameters in PCM-filled single-pass shell and tube heat exchangers. Renew. Energy. https://doi.org/10.1016/j.renene.2016.05.090

Electronic copy available at: https://ssrn.com/abstract=4220792

Sun, X., Liu, L., Mo, Y., Li, J., Li, C., 2020. Enhanced thermal energy storage of a paraffin-based phase change material (PCM) using nano carbons. Appl. Therm. Eng. 181, 115992. https://doi.org/https://doi.org/10.1016/j.applthermaleng.2020.115992

Trp, A., Lenic, K., Frankovic, B., 2006. Analysis of the influence of operating conditions and geometric parameters on heat transfer in water-paraffin shell-and-tube latent thermal energy storage unit. Appl. Therm. Eng. https://doi.org/10.1016/j.applthermaleng.2006.02.004

Voller, V.R., Prakash, C., 1987. A fixed grid numerical modelling methodology for convection-diffusion mushy region phase-change problems. Int. J. Heat Mass Transf. 30, 1709–1719. https://doi.org/https://doi.org/10.1016/0017-9310(87)90317-6

Wazeer, A., Das, A., Abeykoon, C., Sinha, A., Karmakar, A., 2022. Phase change materials for battery thermal management of electric and hybrid vehicles: A review. Energy Nexus 7, 100131. https://doi.org/https://doi.org/10.1016/j.nexus.2022.100131

Yao, L.S., Chen, F.F., 1980. Effects of Natural Convection in the Melted Region Around a Heated Horizontal Cylinder. J. Heat Transfer 102, 667–672. https://doi.org/10.1115/1.3244369

Yazici, M.Y., Avci, M., Aydin, O., Akgun, M., 2014. On the effect of eccentricity of a horizontal tube-in-shell storage unit on solidification of a PCM. Appl. Therm. Eng. https://doi.org/10.1016/j.applthermaleng.2013.12.005

Zhang, S., Feng, D., Shi, L., Wang, L., Jin, Y., Tian, L., Li, Z., Wang, G., Zhao, L., Yan, Y., 2021. A review of phase change heat transfer in shape-stabilized phase change materials (ss-PCMs) based on porous supports for thermal energy storage. Renew. Sustain. Energy Rev. 135, 110127. https://doi.org/https://doi.org/10.1016/j.rser.2020.110127

Zheng, Z.J., Xu, Y., Li, M.J., 2018. Eccentricity optimization of a horizontal shell-and-tube latent-heat thermal energy storage unit based on melting and melting-solidifying performance. Appl. Energy. https://doi.org/10.1016/j.apenergy.2018.03.126

Electronic copy available at: https://ssrn.com/abstract=4220792